

# Multiband Below-Cutoff Propagation in Rectangular Waveguides Filled with Multilayer Left-/Right-Handed Metamaterials

Qianru Weng<sup>1</sup>, Qian Lin<sup>2, \*</sup>, and Haifeng Wu<sup>3</sup>

**Abstract**—An accurate rigorous modal theory has been applied to investigate the propagation characteristics in a rectangular waveguide filled with multilayer left-handed and right-handed metamaterials. It is shown that such a waveguide supports different passbands below the waveguide's cutoff frequency, and the number of passbands is related to the corresponding layers of different left-handed metamaterials (LHMs) filled in the waveguide. The rigorous modal analysis of this structure reveals in detail how the waveguide geometry and left-handed metamaterial parameters may be selected to design rectangular waveguides supporting double or triple below-cutoff passbands. The efficient power transmissions in these below-cutoff passbands are validated by using the full-wave simulation software HFSS. These structures supporting multiple below-cutoff passbands could find applications in waveguide components requiring miniaturization and multiband properties, such as miniaturized multifunctional antennas and filters.

## 1. INTRODUCTION

As 5G research is maturing and continues to support global standardization, researchers have already been engaged in mapping the development tendency of 6G. Thus, mobile terminal devices are required to support multiple networks of 3G and 4G, even 5G and 6G soon [1]. As the critical components in these devices, antennas and filters with multiple operation frequency bands are desired. Moreover, small size and light weight are the key considerations in the design of mobile devices. Therefore, miniaturized multiband components are in great need.

Rectangular waveguides have been used as essential guiding structures in microwaves communications, radars, and antenna technology for almost six decades. Even though planar guiding structures have surpassed rectangular waveguides in many applications and led to miniaturization and integration of microwave systems, rectangular waveguides are still indispensable in the applications requiring high power-handling capability and in the feeding networks for large antenna array [2]. Besides, since the substrate integrated waveguides (SIWs) have been proposed to realize rectangular waveguides on planar structures in the past decade [3], various components based on the rectangular waveguides have come back into the public view.

Electromagnetic waves guided by left-handed metamaterials (LHMs) can exhibit new properties that are not available in natural materials because the permittivity and permeability of LHM are both negative [4]. Filling rectangular waveguides with LHM has been a novel area of research. Counterintuitive propagation characteristics are achieved through filling LHMs in hollow or conventional dielectric filled waveguides. It has been found that a backward wave passband well below the waveguide's cutoff frequency could be created through fully filling LHM in a rectangular waveguide [5].

---

*Received 3 November 2020, Accepted 1 December 2020, Scheduled 4 December 2020*

\* Corresponding author: Qian Lin (linqian@tju.edu.cn).

<sup>1</sup> Schools of Computers, Guangdong University of Technology, Guangzhou, Guangdong 510006, China. <sup>2</sup> College of Physics and Electronic Information Engineer, Qinghai University for Nationalities, Xining 810007, China. <sup>3</sup> Chengdu Ganide Technology, Chengdu 610073, China.

The transversal width of this waveguide can be in principle arbitrarily small. Similar below-cutoff propagation could also be observed in a rectangular waveguide partially filled with LHM. The rest of the waveguide is empty or filled with ordinary material (i.e., right-handed material, RHM) [6–8]. Fully or partially filling the waveguides with LHM can significantly reduce the waveguides' dimensions. Thus, these structures can be used to design miniaturized waveguide components [9, 10].

Creating passbands in a rectangular waveguide below its cutoff frequency is an important way to realize multiband properties. Most of the previous techniques are based on the creation of artificial boundary conditions on the waveguide walls [11]. Filling LHM in the waveguides provides a new way towards this aim. In addition to LHM (i.e., double negative metamaterial, DNG), filling single negative metamaterial (SNG) can also achieve below-cutoff passband in the waveguides [12]. Inspired by this idea, rectangular waveguides supporting double or triple below-cutoff passbands are created by filling two or three LHM layers, respectively [13]. Each LHM layer possesses different dielectric properties. By adjusting LHM properties, the below-cutoff passbands can be targeted at the desired frequencies. However, these papers mainly focus on the physical implementation and application of these multiband structures, without giving the accurate quantitative modal analysis or detailed design process. In this paper, a rigorous modal theory is proposed to accurately determine the cutoff frequency and the dispersion curve of each passband supported by the waveguide. Conversely, to design a rectangular waveguide supporting below-cutoff passbands with targeted cutoff frequencies, the waveguide dimensions and the required LHM properties could be obtained by using the proposed modal theory.

Based on this rigorous modal theory, an arbitrary number of below-cutoff passbands could be generated in principle by filling the corresponding number of different LHM layers in the waveguides without considering the coupling effect between LHM layers. Although in this paper, the property of the fundamental  $LSE_{10}$  mode is mainly discussed, this theory can be used to analyse any longitudinal-section electric (LSE) modes or longitudinal-section magnetic (LSM) modes. Moreover, this theory could be easily extended to other closed metallic waveguides such as cylindrical waveguides [14], elliptical waveguides, or regular polygonal waveguides [15]. The closed-form analytical expressions of the modal fields and eigenequations for LSE and LSM modes are derived in Section 2. Section 3 offers detailed design processes for rectangular waveguides filled with LHM layers supporting single or double below-cutoff passbands. Section 4 presents the dispersion diagrams of these waveguides. The full-wave transmission simulations show good consistency with the theoretical results and validate efficient power transmission in these below-cutoff passbands. Section 5 extends the modal theory to design a rectangular waveguide supporting triple below-cutoff passbands. Section 6 is the conclusion.

## 2. RIGOROUS MODAL THEORY

Figure 1 shows the cross-section of a rectangular waveguide consisting of three regions. Region#1 and Region#3 are filled with LHMs, and Region#2 is filled with ordinary RHM. These regions are characterized by the thickness  $d_t$ , permittivity  $\epsilon_t = \epsilon_{rt}\epsilon_0$ , and permeability  $\mu_t = \mu_{rt}\mu_0$  ( $t = 1, 2, 3$ ). The modes in this rectangular waveguide are classified as the longitudinal section electric (LSE) and the

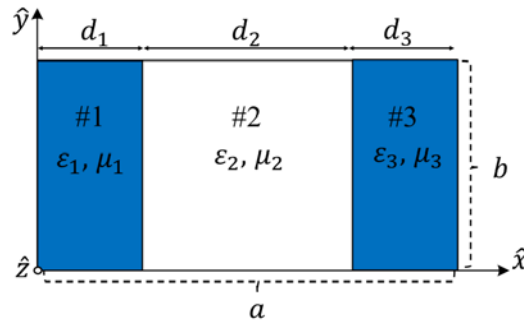


**Figure 1.** The cross-section of a three-region rectangular waveguide filled with LHM in Region#1 and Region#3.

longitudinal section magnetic (LSM) modes [16]. The closed-form eigenequations of LSE<sub>mn</sub> and LSM<sub>mn</sub> modes are derived analytically by applying appropriate boundary conditions to Maxwell equations. This structure is assumed to be uniform along the  $z$ -direction, and  $z$  is chosen as the direction of the wave propagation. Hence the  $z$  variation has the form  $e^{-\gamma z}$  (the time-harmonic variation  $e^{j\omega t}$  is assumed throughout).

For LSE<sub>mn</sub> modes ( $E_x = 0$ ), the analytical electric- and magnetic-field expressions in Region# $t$  ( $t = 1, 2, 3$ ) are written as:

Region#1

$$E_{1y} = j\omega\mu_1\gamma A_1 \sin(k_1x) \cos\left(\frac{n\pi y}{b}\right) \quad (1a)$$

$$E_{1z} = -j\omega\mu_1 \left(\frac{n\pi}{b}\right) A_1 \sin(k_1x) \sin\left(\frac{n\pi y}{b}\right) \quad (1b)$$

$$H_{1x} = \left[\left(\frac{n\pi}{b}\right)^2 - \gamma^2\right] A_1 \sin(k_1x) \cos\left(\frac{n\pi y}{b}\right) \quad (1c)$$

$$H_{1y} = -\left(\frac{n\pi}{b}\right) k_1 A_1 \cos(k_1x) \sin\left(\frac{n\pi y}{b}\right) \quad (1d)$$

$$H_{1z} = -\gamma k_1 A_1 \cos(k_1x) \cos\left(\frac{n\pi y}{b}\right) \quad (1e)$$

Region#2

$$E_{2y} = j\omega\mu_2\gamma [A_2 \sin(k_2x) + B_2 \cos(k_2x)] \cos\left(\frac{n\pi y}{b}\right) \quad (2a)$$

$$E_{2z} = -j\omega\mu_2 \left(\frac{n\pi}{b}\right) [A_2 \sin(k_2x) + B_2 \cos(k_2x)] \sin\left(\frac{n\pi y}{b}\right) \quad (2b)$$

$$H_{2x} = \left[\left(\frac{n\pi}{b}\right)^2 - \gamma^2\right] [A_2 \sin(k_2x) + B_2 \cos(k_2x)] \cos\left(\frac{n\pi y}{b}\right) \quad (2c)$$

$$H_{2y} = -\left(\frac{n\pi}{b}\right) k_2 [A_2 \cos(k_2x) - B_2 \sin(k_2x)] \sin\left(\frac{n\pi y}{b}\right) \quad (2d)$$

$$H_{2z} = -\gamma k_2 [A_2 \cos(k_2x) - B_2 \sin(k_2x)] \cos\left(\frac{n\pi y}{b}\right) \quad (2e)$$

Region#3

$$E_{3y} = j\omega\mu_3\gamma A_3 \sin(k_3(a-x)) \cos\left(\frac{n\pi y}{b}\right) \quad (3a)$$

$$E_{3z} = -j\omega\mu_3 \left(\frac{n\pi}{b}\right) A_3 \sin(k_3(a-x)) \sin\left(\frac{n\pi y}{b}\right) \quad (3b)$$

$$H_{3x} = \left[\left(\frac{n\pi}{b}\right)^2 - \gamma^2\right] A_3 \sin(k_3(a-x)) \cos\left(\frac{n\pi y}{b}\right) \quad (3c)$$

$$H_{3y} = \left(\frac{n\pi}{b}\right) k_3 A_3 \cos(k_3(a-x)) \sin\left(\frac{n\pi y}{b}\right) \quad (3d)$$

$$H_{3z} = \gamma k_3 A_3 \cos(k_3(a-x)) \cos\left(\frac{n\pi y}{b}\right) \quad (3e)$$

where  $A_t$  and  $B_t$  ( $t = 1, 2, 3$ ) are the amplitude coefficients;  $k_t^2 = \varepsilon_{rt}\mu_{rt}k_0^2 - \gamma^2 - (n\pi/b)^2$  is the wavenumber in Region# $t$ ;  $k_0^2 = \varepsilon_0\mu_0\omega^2$  is the free space wavenumber;  $\gamma = j\beta$  is the axial propagation constant. According to the boundary conditions,  $E_z$  and  $H_y$  need to be continuous at the interface  $x_t$  and then eliminating all the amplitude coefficients  $A_t$  and  $B_t$ . The closed-form eigenequations of the LSE<sub>mn</sub> mode could be obtained:

$$\sum_{i=1}^3 \frac{\mu_i}{k_i} \tan k_i d_i - \frac{\mu_1\mu_3 k_2}{\mu_2 k_1 k_3} \tan k_1 d_1 \tan k_2 d_2 \tan k_3 d_3 = 0 \quad (4)$$

For LSM<sub>mn</sub> modes ( $H_x = 0$ ), the analytical electric- and magnetic-field expressions in Region# $t$  ( $t = 1, 2, 3$ ) have the following forms:

Region#1

$$E_{1x} = \left[ \left( \frac{n\pi}{b} \right)^2 - \gamma^2 \right] A_1 \cos(k_1 x) \sin\left(\frac{n\pi y}{b}\right) \quad (5a)$$

$$E_{1y} = -\left(\frac{n\pi}{b}\right) k_1 A_1 \sin(k_1 x) \cos\left(\frac{n\pi y}{b}\right) \quad (5b)$$

$$E_{1z} = \gamma k_1 A_1 \sin(k_1 x) \sin\left(\frac{n\pi y}{b}\right) \quad (5c)$$

$$H_{1y} = -j\omega\varepsilon_1 \gamma A_1 \cos(k_1 x) \sin\left(\frac{n\pi y}{b}\right) \quad (5d)$$

$$H_{1z} = -j\omega\varepsilon_1 \left(\frac{n\pi}{b}\right) A_1 \cos(k_1 x) \cos\left(\frac{n\pi y}{b}\right) \quad (5e)$$

Region#2

$$E_{2x} = \left[ \left( \frac{n\pi}{b} \right)^2 - \gamma^2 \right] [A_2 \cos(k_2 x) + B_2 \sin(k_2 x)] \sin\left(\frac{n\pi y}{b}\right) \quad (6a)$$

$$E_{2y} = \left(\frac{n\pi}{b}\right) k_2 [-A_2 \sin(k_2 x) + B_2 \cos(k_2 x)] \cos\left(\frac{n\pi y}{b}\right) \quad (6b)$$

$$E_{2z} = -\gamma k_2 [-A_2 \sin(k_2 x) + B_2 \cos(k_2 x)] \sin\left(\frac{n\pi y}{b}\right) \quad (6c)$$

$$H_{2y} = -j\omega\varepsilon_2 \gamma [A_2 \cos(k_2 x) + B_2 \sin(k_2 x)] \sin\left(\frac{n\pi y}{b}\right) \quad (6d)$$

$$H_{2z} = -j\omega\varepsilon_2 \left(\frac{n\pi}{b}\right) [A_2 \cos(k_2 x) + B_2 \sin(k_2 x)] \cos\left(\frac{n\pi y}{b}\right) \quad (6e)$$

Region#3

$$E_{3x} = \left[ \left( \frac{n\pi}{b} \right)^2 - \gamma^2 \right] A_3 \cos(k_3 (a - x)) \sin\left(\frac{n\pi y}{b}\right) \quad (7a)$$

$$E_{3y} = \left(\frac{n\pi}{b}\right) k_3 A_3 \sin(k_3 (a - x)) \cos\left(\frac{n\pi y}{b}\right) \quad (7b)$$

$$E_{3z} = -\gamma k_3 A_3 \sin(k_3 (a - x)) \sin\left(\frac{n\pi y}{b}\right) \quad (7c)$$

$$H_{3y} = -j\omega\varepsilon_3 \gamma A_3 \cos(k_3 (a - x)) \sin\left(\frac{n\pi y}{b}\right) \quad (7d)$$

$$H_{3z} = -j\omega\varepsilon_3 \left(\frac{n\pi}{b}\right) A_3 \cos(k_3 (a - x)) \cos\left(\frac{n\pi y}{b}\right) \quad (7e)$$

Then eliminating the amplitude coefficients  $A_t$  and  $B_t$ , the dispersion relation of the LSM<sub>mn</sub> mode could be obtained:

$$\sum_{i=1}^3 \frac{k_i}{\varepsilon_i} \tan k_i d_i - \frac{\varepsilon_2 k_1 k_3}{\varepsilon_1 \varepsilon_3 k_2} \tan k_1 d_1 \tan k_2 d_2 \tan k_3 d_3 = 0 \quad (8)$$

The propagation constant  $\gamma$  of the LSE<sub>mn</sub> or LSM<sub>mn</sub> modes is obtained by solving the transcendental closed-form eigenequations (4) or (8). At the cutoff wavenumber, the propagation constant  $\gamma$  has to approach zero, and the cutoff wavenumber results in  $k_{ci}^2 = \varepsilon_{ri} \mu_{ri} k_0^2 - (n\pi/b)^2$ .

The relationships of different characteristics (cutoff frequency and dispersion diagram) versus various LHM dielectric and geometric parameters could be accurately obtained since the eigenequations are in functions of these parameters. One practical application of this rigorous theory are to accurately investigate the temperature influence on the propagation characteristics of rectangular waveguides filled with temperature-sensitive metamaterials, since the temperature model versus metamaterials' geometric and dielectric parameters has been established [17, 18].

### 3. DESIGN PROCESS

In order to extend the results for general use, the solution data in this paper are normalized for all length scales. Therefore, to study the multiband phenomena in such a rectangular waveguide, one may

scale a system from microwave to the optical wave. Since the fundamental mode is the most widely used in various applications, this paper focuses on the characteristics of the LSE<sub>10</sub> mode.

### 3.1. Symmetric Waveguide Structure

A symmetric waveguide structure shown in Fig. 2 is under investigation. In order to reduce the coupling effect between the dielectric slabs, thin dielectric slabs are chosen in this paper,  $d_1/a = d_3/a = 0.05$ . Region#1 and Region#3 are filled with the identical dielectrics possessing  $\epsilon_{r1} = \epsilon_{r3}$  and  $\mu_{r1} = \mu_{r3}$ . Region#2 is filled with ordinary RHM possessing  $\epsilon_{r2} = \mu_{r2} = 1$ . In Fig. 2, the relationship between the normalized cutoff wavenumber of the LSE<sub>10</sub> mode ( $k_c a$ ) and the relative permittivity  $\epsilon_{r1}$  is shown. The cutoff relations are obtained by using the closed-form eigenequation (4) through applying the cutoff condition  $\gamma = 0$ .

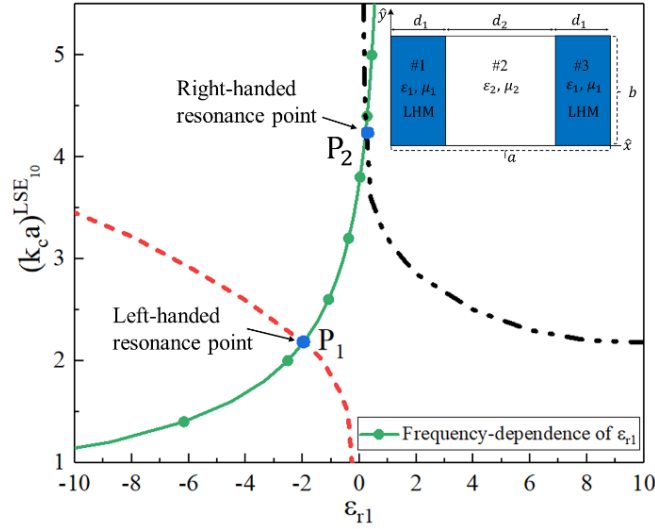


**Figure 2.** The normalized cutoff wavenumbers  $k_c a$  for LSE<sub>10</sub> mode versus the permittivity  $\epsilon_{r1}$  (red dash line for  $\epsilon_{r1} > 0$ , and black dash-dot line for  $\epsilon_{r1} < 0$ ). The waveguide’s dimensions are  $a = 1$ ,  $b = 0.5$ , and  $d_1/a = d_3/a = 0.05$ . The frequency response of the LHM  $\epsilon_{r1}(\omega)$  (solid green circle) is described by the normalized Drude model parameters  $\omega_{pe} = \omega_{pm} = 3.749$  and  $\Gamma_e = \Gamma_m = 0$ .

On the right side of Fig. 2,  $\epsilon_{r1} > (\mu_{r1} > 0)$  indicates that the materials filled in Region#1 and Region#3 are the ordinary RHMs. The cutoff wavenumber’s dependence on the positive permittivity ( $\epsilon_{r1}$ ) values as shown in Fig. 2 (black dash-dot line) is consistent with the well-known results: filling a rectangular waveguide by RHM slabs with permittivity larger than unity lowers the waveguide’s cutoff wavenumber [16]. However, the cutoff frequency increases significantly when the values of positive permittivity are smaller than unity [14, 19]. On the left side of Fig. 2,  $\epsilon_{r1} < (\mu_{r1} < 0)$  indicates that Region#1 and Region#3 are filled with LHMs. The cutoff wavenumber’s dependence on negative permittivity values (red dashed line in Fig. 2) is different from that of positive permittivity: negative permittivity with larger than unity produces decreased cutoff wavenumbers [20]. If the negative permittivity value of LHM slabs is smaller than unity, the cutoff wavenumbers of the LSE<sub>10</sub> mode is dramatically lowered [14, 21]. In Fig. 2, there is an implicit premise that the metamaterial’s permittivity ( $\epsilon_{r1}$ ) could be achieved at the desired cutoff frequency.

It is well known that the frequency-dependence (dispersion) is a crucial and nonnegligible characteristic of LHM [20], and several frequency response modals for LHM have been proposed. In this paper, the frequency response of LHM must be considered in the modal analysis. The permittivity and permeability of LHM could be described by the Drude model:

$$\epsilon_r(\omega) = \left[ 1 - \frac{\omega_{pe}^2}{\omega(\omega + i\Gamma_e)} \right] \tag{9a}$$

$$\mu_r(\omega) = \left[ 1 - \frac{\omega_{pm}^2}{\omega(\omega + i\Gamma_m)} \right] \quad (9b)$$

in which  $\omega_{pe}$  and  $\omega_{pm}$  are the plasma frequencies, and  $\Gamma_e$  and  $\Gamma_m$  are the damping constants representing LHM's tangent losses. The Drude model can yield a negative real part of the permittivity and permeability over a wide frequency range ( $\omega < \sqrt{\omega_p^2 - \Gamma^2}$ ) [20]. This model accurately approximates the dispersion response of LHM over the investigated frequency range.

For this symmetric rectangular waveguide, the waveguide dimensions are chosen as  $a = 1$ ,  $b = 0.5$ . In Fig. 2, an LHM permittivity of  $\varepsilon_{r1} = -2$  will lead to a reduced normalized cutoff wavenumber of  $k_c a = 2.199$ . To achieve this cutoff wavenumber, the dispersive permeability  $\varepsilon_{r1}$  and dispersive permittivity  $\mu_{r1}$  of LHM are enforced to have the same frequency-dependent response, and the normalized Drude model parameters for the LHM are set to  $\omega_{pe} = \omega_{pm} = 3.749$  and  $\Gamma_e = \Gamma_m = 0$ . Superposing the LHM's dispersive permittivity curve (solid green circle) on the cutoff-wavenumber relation curve in Fig. 2, two intersections are obtained: the lower intersection  $P_1(\varepsilon_{r1}, k_c a) = (-2, 2.199)$  corresponds to the left-handed resonance point, which is also the desired LSE<sub>10</sub>-mode cutoff wavenumber; the higher intersection  $P_2(\varepsilon_{r1}, k_c a) = (0.203, 4.25)$  corresponds to the right-handed resonance point. These two intersections refer to two cutoff wavenumbers of the fundamental LSE<sub>10</sub> mode. Thus, this waveguide supports dual-band operation. One passband is below the waveguide's cutoff wavenumber, and the other passband is above the cutoff wavenumber. The bandgap between these two intersections is 2.051. The dispersion diagram and full-wave simulation of this structure are presented in Section 4.

### 3.2. Asymmetric Waveguide Structure

An asymmetric waveguide structure as shown in Fig. 3 is investigated. Region#1 and Region#3 are filled with different dielectrics having  $\varepsilon_{r1} = \kappa\varepsilon_{r3}$  ( $\kappa > 0$  and  $\kappa$  is real) and  $\mu_{r1} = \mu_{r3}$ . Region#2 is filled with an ordinary RHM having  $\varepsilon_{r2} = \mu_{r2} = 1$ . The waveguide's dimensions are still chosen as  $a = 1$ ,  $b = 0.5$ , and  $d_1/a = d_3/a = 0.05$ . Letting  $\kappa = 0.5$ , the relationship between  $k_c a$  of the LSE<sub>10</sub> mode

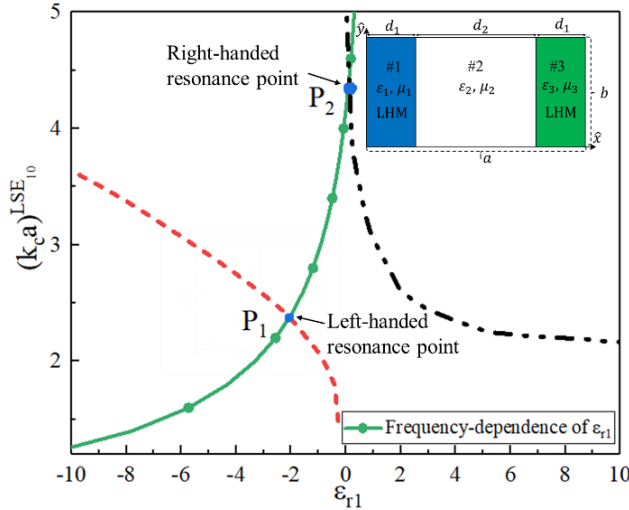


**Figure 3.** The normalized cutoff wavenumber  $k_c a$  of LSE<sub>10</sub> mode versus the permittivity  $\varepsilon_{r1}$  in Region#1,  $\kappa = 0.5$  (red dash line for  $\varepsilon_{r1} > 0$ , and black dash-dot line for  $\varepsilon_{r1} < 0$ ). The waveguide's dimensions are  $a = 1$ ,  $b = 0.5$ , and  $d_1/a = d_3/a = 0.05$ . The normalized Drude model parameters for  $\varepsilon_{r1}(\omega)$  are  $\omega_{pe} = \omega_{pm} = 4.15$  and  $\Gamma_e = \Gamma_m = 0$  (solid green circle).

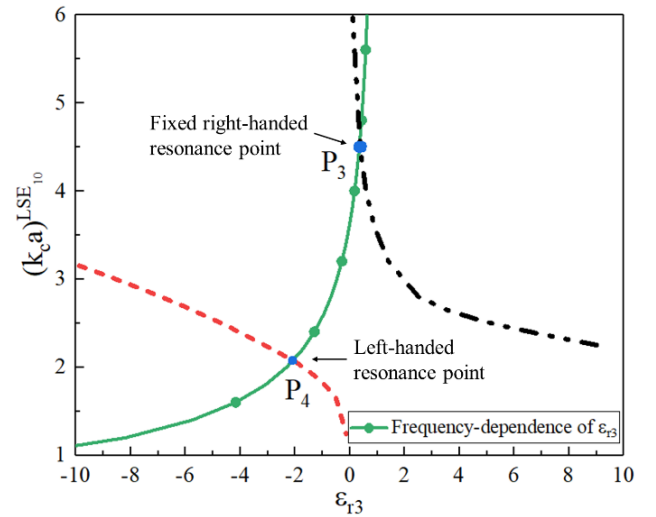


**Figure 4.** The normalized cutoff wavenumber  $k_c a$  of LSE<sub>10</sub> mode versus the permittivity  $\varepsilon_{r3}$  in Region#3 (red dash line for  $\varepsilon_{r3} > 0$ , and black dash-dot line for  $\varepsilon_{r3} < 0$ ),  $\varepsilon_{r1} = -2$ . The normalized Drude model parameters for  $\varepsilon_{r3}(\omega)$  are  $\omega_{pe} = \omega_{pm} = 3.635$  and  $\Gamma_e = \Gamma_m = 0$ .

and the relative permittivity  $\varepsilon_{r1}$  is shown in Fig. 3, which is also calculated from the eigenequation (4) ( $\gamma = 0$ ). It can be observed from Fig. 3 that  $\varepsilon_{r1} = -2$  of the LHM permittivity in Region#1 corresponds to a reduced cutoff wavenumber of  $k_c a = 2.382$ . Similarly, to achieve this desired cutoff wavenumber, enforcing the permeability and permittivity of the LHM possessing the same dispersion response, the normalized Drude model parameters for the LHM in Region#1 are set to  $\omega_{pe} = \omega_{pm} = 4.15$  and  $\Gamma_e = \Gamma_m = 0$ . Superposing the LHM's dispersive response (solid green circle) on the cutoff-wavenumber curve as shown in Fig. 3, two intersections are observed: the lower left-handed resonance intersection  $P_1(\varepsilon_{r1}, k_c a) = (-2, 2.382)$  corresponding to the designed LSE<sub>10</sub>-mode cutoff; the higher right-handed resonance intersection  $P_2(\varepsilon_{r1}, k_c a) = (0.205, 4.448)$ .

Then, since the permittivity in Region#1 is set to  $\varepsilon_{r1} = -2$ , the relationship between the normalized cutoff wavenumber  $k_c a$  for LSE<sub>10</sub> mode and the relative permittivity  $\varepsilon_{r3}$  in Region#3 is shown in Fig. 4. To obtain the Drude modal parameters, the cutoff wavenumber of the right-handed resonance point is fixed to  $k_c a = 4.448$ . From the relationship between  $k_c a$  and  $\varepsilon_{r3}$  in Fig. 4,  $k_c a = 4.448$  will result in a relative permittivity  $\varepsilon_{r3} = 0.32$ . Thus, the normalized Drude model parameters could be set to  $\omega_{pe} = \omega_{pm} = 3.635$  and  $\Gamma_e = \Gamma_m = 0$ . Superposing the Drude model curve of the relative dispersive permittivity  $\varepsilon_{r3}$  (solid green circle) on the cutoff-wavenumber curve, as shown in Fig. 4, two intersections are observed: the higher intersection  $P_3(\varepsilon_{r3}, k_c a) = (0.32, 4.48)$  corresponds to the fixed right-handed resonance point, and the lower intersection  $P_4(\varepsilon_{r3}, k_c a) = (-2.12, 2.071)$ .

Since each of intersections corresponds to a cutoff frequency, this asymmetric waveguide supports three passbands: two passbands below the waveguide's cutoff wavenumber which is located at  $k_c a^{P1} = 2.382$  and  $k_c a^{P4} = 2.071$ , and one passband above the waveguide's cutoff wavenumber because  $k_c a^{P2} = k_c a^{P3} = 4.448$ . The dispersion diagram of this waveguide structure is presented in Section 4.

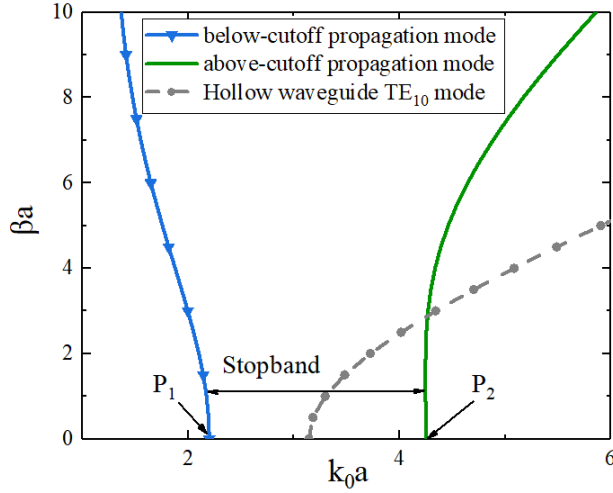
In this section, the detailed design procedure for rectangular waveguides supporting single or double below-cutoff passbands is proposed. The design process can be concluded as a general manner, which could be applied to design waveguide supporting arbitrary number of below-cutoff passbands. Firstly, the accurate relationships between the cutoff frequency and the permittivity are obtained by using the rigorous modal theory. Secondly, the required waveguide dimension and permittivity for a targeted cutoff frequency is determined according to the cutoff relationships. Thirdly, various parameters of the dispersion modal for the filled dielectric could be determined. Finally, superposing the dispersion curve of the dielectrics on the cutoff relationships, the cutoff frequencies of the passbands could be obtained. In Section 5, this design process has been extended to design a rectangular waveguide supporting triple below-cutoff passbands.

From the above design procedure, only the cutoff frequency of each passband is obtained. To clearly possess the propagation characteristics in each passband, the dispersion diagrams of waveguides supporting single and double below-cutoff passbands are calculated from the rigorous modal theory in Section 4. The full-wave simulation validation of these passbands is also presented in the following section.

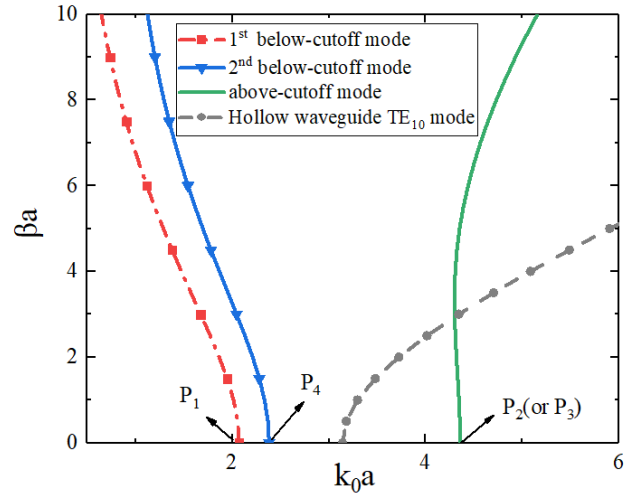
#### 4. DISPERSION DIAGRAMS AND FULL-WAVE SIMULATION VALIDATION

Figure 5 presents the normalized LSE<sub>10</sub>-mode dispersion diagram of a rectangular waveguide symmetrically filled with the identical LHM in Region#1 and Region#3. The cutoff wavenumber of each passband is determined from Fig. 2. As suggested from the two intersections ( $P_1, P_2$ ) in Fig. 2, such a waveguide supports two propagating bands: a passband above the waveguide's cutoff wavenumber and a frequency-reduced passband below its cutoff frequency. In Fig. 5, the above-cutoff dispersion curve (green solid line) exhibits positive group velocity ( $\partial\omega/\partial\beta > 0$ ), suggesting that forward wave propagates in this passband. The below-cutoff dispersion curve (blue solid triangle) shows negative group velocity ( $\partial\omega/\partial\beta < 0$ ), indicating the backward wave propagation. Backward wave propagation in the below-cutoff passband has been experimentally verified in [5, 14].

As shown for comparison, the fundamental TE<sub>10</sub>-mode dispersion diagram of a hollow rectangular waveguide with same dimensions is also presented in Fig. 5 (solid grey circles). The normalized cutoff wavenumber of this hollow waveguide is  $k_0 a = 3.14$ , which is higher than that of below-cutoff passband. Besides, the group velocities of the above-cutoff and below-cutoff propagation modes (almost constant,  $\partial\omega/\partial\beta \sim \text{constant}$ ) are much lower than that of TE<sub>10</sub> mode in the hollow waveguide. This interesting



**Figure 5.** Dispersion diagram for LSE<sub>10</sub> mode in a rectangular waveguide symmetrically filled the identical LHM in Region#1 and Region#3.



**Figure 6.** Dispersion diagram for LSE<sub>10</sub> mode in an asymmetric rectangular waveguide filled with different LHMs in Region#1 and Region#3.

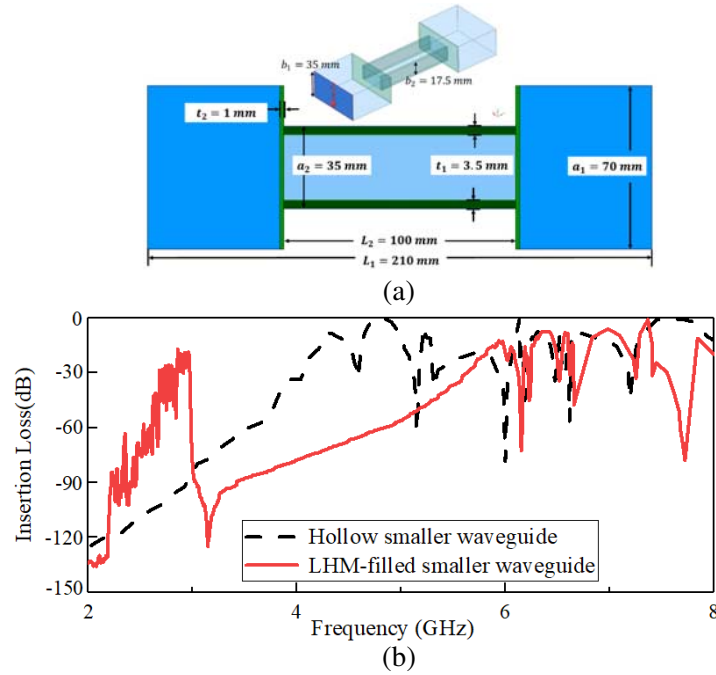
phenomenon indicates that a waveguide filled with LHM may support slow wave propagation. However, the slow wave propagation needs further verification, which will be conducted in the future investigation.

Figure 6 presents the LSE<sub>10</sub>-mode dispersion diagram of a rectangular waveguide asymmetrically filled with different LHMs in Region#1 and Region#3, and the cutoff wavenumbers are determined from Fig. 3 and Fig. 4. As suggested from three intersections in Fig. 3 and Fig. 4, such a waveguide supports two passbands well below its cutoff frequency and one above-cutoff passband. In Fig. 6, the two below-cutoff dispersion curves show negative group velocity ( $\partial\omega/\partial\beta < 0$ ), indicating the backward wave propagation. These two curves are very close to each other, and the slopes of these curves are steep, indicating that these two below-cutoff passbands have narrow bandwidths.

The dispersion diagrams of waveguides supporting single or double below-cutoff passbands show the propagation characteristics in these structures. However, only dispersion diagram is insufficient to verify the effective power transmission in the below-cutoff passbands. Moreover, it is necessary to verify the theoretic results obtained by the rigorous modal theory by using the full-wave simulation software. Therefore, a transmission analysis is conducted by using the finite element simulator ANSYS HFSS on the simulation model shown as Fig. 7(a). In this structure setup, the TE<sub>10</sub>-mode's cutoff frequency of two-larger hollow rectangular waveguides with identical geometry dimensions  $a_1 = 70$  mm and  $b_1 = 35$  mm is 2.142 GHz. These two-larger waveguides are connected by a smaller hollow rectangular waveguide. The geometry dimensions of smaller waveguides are  $a_2 = 35$  mm and  $b_2 = 17.5$  mm, possessing a fundamental TE<sub>10</sub> mode with cutoff frequency of 4.284 GHz. Wave ports are placed at each end of the larger waveguides. The dashed black curve in Fig. 7(b) shows the insertion loss of this structure setup. The insertion loss is higher than  $-10$  dB above 4.284 GHz, and the power transmits efficiently in this region. The insertion loss below 4.284 GHz decreases rapidly. It is verified that the intermediate smaller waveguide only supports one passband above its cutoff frequency 4.284 GHz.

Then, two identical LHM slabs of thicknesses  $t_1 = 3.5$  mm are filled next to the walls in the hollow small rectangular waveguide, possessing the dispersive Drude model parameters  $\epsilon_{r1}(\omega)$  determined by the design process in Section 3. At the junctions between the larger rectangular waveguides and the small rectangular waveguide, square dielectric rings possessing the same dielectric properties as LHM are placed to enhance the coupling of the electromagnetic modes between the different sizes rectangular waveguides [14, 21].

According to the rigorous modal theory presented in Section 3, for the proposed rectangular waveguide filled with two identical LHM slabs, transmission should occur below 3.001 GHz for a single below-cutoff passband and above 5.798 GHz for an above-cutoff passband. The insertion loss of this structure is presented as the solid red curve in Fig. 7(b). There are two passbands: a passband



**Figure 7.** (a) HFSS simulation geometry setup for the transmission validation; (b) insertion losses for the hollow smaller structure (dashed black curve), and for LHM-filled smaller rectangular waveguide (solid red curve).

below 3.001 GHz, which follows the theoretical result of the below-cutoff passband; a passband above 5.798 GHz, which follows the theoretical result of the above-cutoff passband. Thus, the cutoff frequencies of the multiple passbands predicted by the rigorous modal theory are in accordance with the HFSS simulation results. The insertion losses in the below-cutoff passband and the above-cutoff passband are both higher than  $-15\text{ dB}$ , indicating that both passbands can transmit power efficiently.

### 5. TRIPLE BELOW-CUTOFF PASSBANDS REALIZATION

According to the general design process described in Section 3, a triple-passband configuration could be realized by adding a middle LHM slab in the previous asymmetric structure. As shown in Fig. 8, Region#1, Region#3, and Region#5 are filled with dielectrics possessing different permittivities  $\epsilon_{r1} = \kappa_1 \epsilon_{r3} = \kappa_2 \epsilon_{r5}$  ( $\kappa_1, \kappa_2 > 0$ ,  $\kappa_1$  and  $\kappa_2$  are real) and  $\mu_{r1} = \mu_{r3} = \mu_{r5}$ , and Region#2 and Region#4 are filled with RHM with  $\epsilon_{r2} = \epsilon_{r4} = \mu_{r2} = \mu_{r4} = 1$ . The waveguide’s dimensions are  $a = 1$ ,  $b = 0.5$ , and  $d_1/a = d_3/a = d_5/a = 0.05$ .

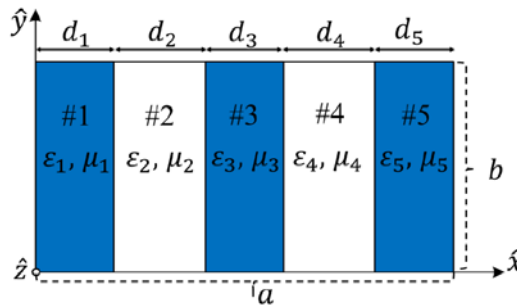


**Figure 8.** The cross-section of a five-region rectangular waveguide filled with two different LHM slabs on each wall and a middle LHM slab.

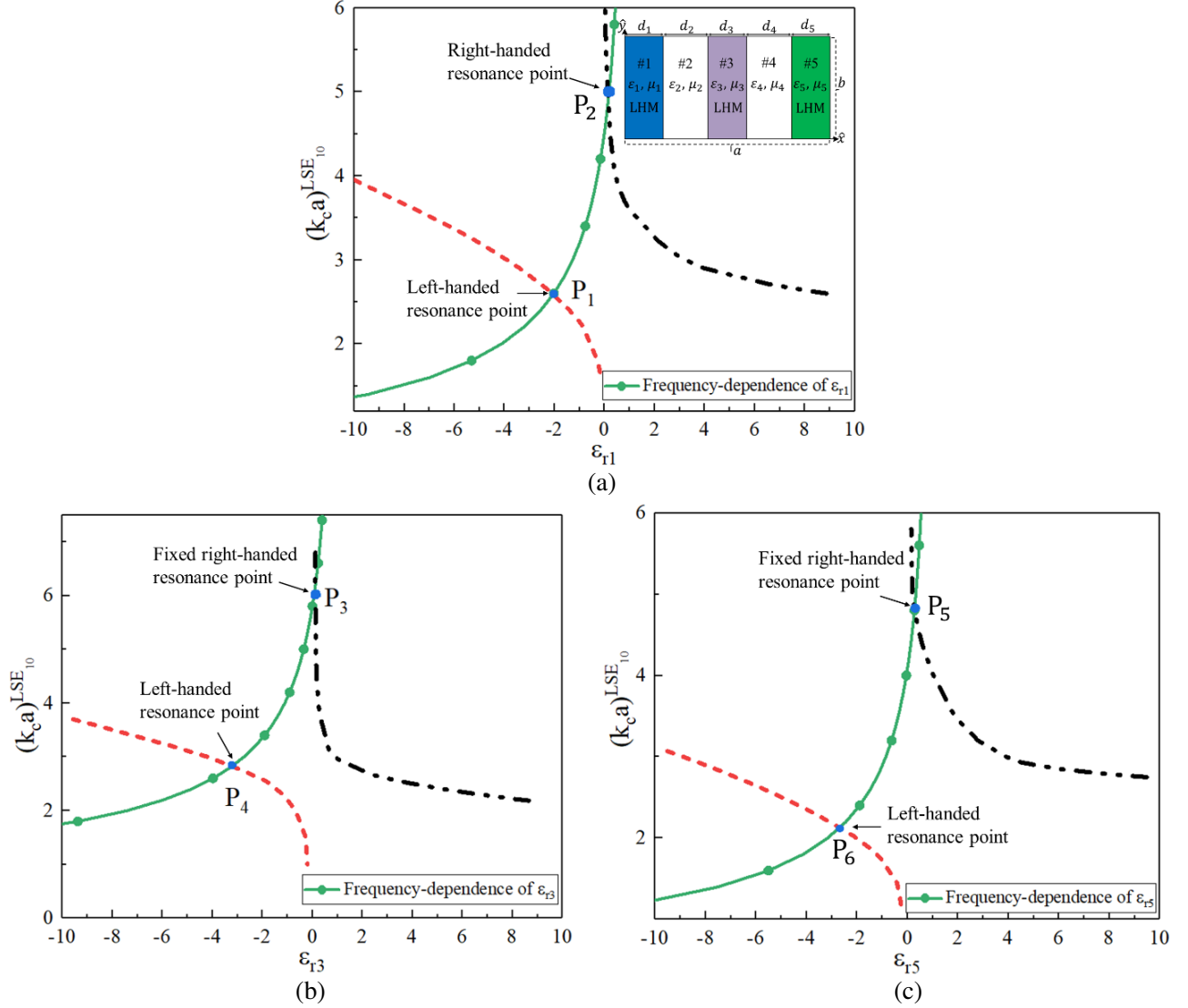


**Figure 9.** (a) The normalized cutoff wavenumber  $k_c a$  of  $LSE_{10}$  mode versus the permittivity  $\epsilon_{r1}$  in Region#1,  $\kappa_1 = 2/3$  and  $\kappa_2 = 1/2$ ; (b) the normalized cutoff wavenumber  $k_c a$  of  $LSE_{10}$  mode versus the permittivity  $\epsilon_{r3}$  in Region#3,  $\epsilon_{r1} = -2$ , and  $\kappa_2 = 1/2$ ; (c) the normalized cutoff wavenumber  $k_c a$  of  $LSE_{10}$  mode versus the permittivity  $\epsilon_{r5}$  in Region#5,  $\epsilon_{r1} = -2$  and  $\epsilon_{r3} = -3$ .

Assuming  $\kappa_1 = 2/3$  and  $\kappa_2 = 1/2$ , the relationship between the normalized  $LSE_{10}$  mode cutoff wavenumber  $k_c a$  and the relative permittivity  $\epsilon_{r1}$  is shown in Fig. 9(a), where red dashed line is for  $\epsilon_{r1} > 0$  and black dash-dot line for  $\epsilon_{r1} < 0$ . It can be observed from Fig. 9(a) that an LHM permittivity  $\epsilon_{r1} = -2$  will result in a reduced cutoff wavenumber of  $k_c a = 2.621$ . Thus, the normalized Drude model parameters for the LHM are set to  $\omega_{pe} = \omega_{pm} = 4.520$  and  $\Gamma_e = \Gamma_m = 0$ . Superposing the dispersive permittivity  $\epsilon_{r1}(\omega)$  (solid green circle) on the cutoff curve in Fig. 9(a), two intersections are obtained: the lower intersection  $P_1(\epsilon_{r1}, k_c a) = (-2, 2.621)$  corresponds to the left-handed resonance point; the higher intersection  $P_2(\epsilon_{r1}, k_c a) = (0.227, 4.881)$  corresponds to the right-handed resonance point.

Letting that  $\epsilon_{r1} = -2$  and  $\kappa_2 = 1/2$ , the relationship between the normalized cutoff wavenumber of the  $LSE_{10}$  mode  $k_c a$  and the relative permittivity  $\epsilon_{r3}$  is shown in Fig. 9(b), where red dashed line is for  $\epsilon_{r3} > 0$  and black dash-dot line for  $\epsilon_{r3} < 0$ . The right-handed resonance point is fixed to  $k_c a = 4.881$ . It can be observed from Fig. 9(b) that  $k_c a = 4.881$  will result in a permittivity  $\epsilon_{r3} = 0.387$ . The normalized Drude model parameters are set to  $\omega_{pe} = \omega_{pm} = 3.821$  and  $\Gamma_e = \Gamma_m = 0$ . Superposing the dispersive curve  $\epsilon_{r3}(\omega)$  (solid green circle) on the cutoff curve in Fig. 9(b), two intersections are observed: the

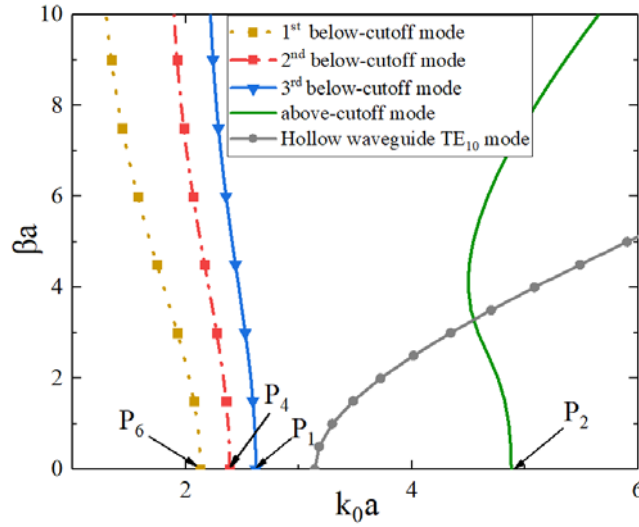


**Figure 10.** Dispersion diagram for LSE<sub>10</sub> mode in a rectangular waveguide supporting triple below-cutoff passbands.

higher intersection  $P_3(\varepsilon_{r3}, k_c a) = (0.387, 4.881)$ ; the lower intersection  $P_4(\varepsilon_{r3}, k_c a) = (-1.47, 2.39)$ .

Finally, assuming  $\varepsilon_{r1} = -2$  and  $\varepsilon_{r3} = -3$ , the relationship between the normalized cutoff wavenumber of the LSE<sub>10</sub> mode  $k_c a$  and the relative permittivity  $\varepsilon_{r5}$  is shown in Fig. 9(c), where red dashed line is for  $\varepsilon_{r5} > 0$  and black dash-dot line for  $\varepsilon_{r5} < 0$ . The right-handed resonance point is also fixed to  $k_c a = 4.881$ . It can be observed from Fig. 9(c) that  $k_c a = 4.881$  will result in a permittivity  $\varepsilon_{r5} = 301$ . Thus, the normalized Drude model parameters are set to  $\omega_{pe} = \omega_{pm} = 4.081$  and  $\Gamma_e = \Gamma_m = 0$ . Superposing the dispersive curve (solid green circle) on the cutoff curve in Fig. 9(c), two intersections are observed: the higher intersection  $P_5(\varepsilon_{r5}, k_c a) = (0.301, 4.881)$ ; the lower intersection  $P_6(\varepsilon_{r5}, k_c a) = (-2.67, 2.13)$ .

Since each of these intersections corresponds to a cutoff frequency for one of the passbands, there are three different below-cutoff passbands located at  $k_c a^{P1} = 2.621$ ,  $k_c a^{P4} = 2.39$ , and  $k_c a^{P6} = 2.13$ . This structure also supports a above-cutoff passband because  $k_c a^{P2} = k_c a^{P3} = k_c a^{P5} = 4.881$ . The dispersion diagram of this triple below-cutoff passbands structure is presented in Fig. 10. The dispersion curves of the three below-cutoff propagation modes exhibit negative group velocity ( $\partial\omega/\partial\beta < 0$ ), indicating the backward wave propagation. These three dispersion curves are very close to each other, and the slopes of these curves are steep, showing that the bandwidths of three below-cutoff passbands are narrow. Compared with the dispersion curves of the fundamental TE<sub>10</sub>-mode in a hollow rectangular waveguide, the group velocity ( $\partial\omega/\partial\beta$ ) in this waveguide supporting triple below-cutoff passbands changes very slowly, indicating that such a structure might support slow-wave propagation.

## 6. CONCLUSION

In this paper, a rigorous modal theory combining with the dispersion nature of the LHM has been used to accurately determine the cutoff and propagation characteristics in a rectangular waveguide filled with multilayer left-handed metamaterials (or composite left-handed and right-handed metamaterials). It has been shown that such a waveguide supports multiple passbands well below the waveguide's cutoff frequency. A general design process based on the rigorous modal theory for multiband waveguides has been concluded, and an arbitrary number of below-cutoff bands could be generated in principle by filling corresponding number of different LHMs in the waveguides. Waveguides supporting single, double, and triple below-cutoff passbands are designed as examples. Full-wave simulation results of the transmission properties show that the power transmits efficiently in these below-cutoff passbands. The presented structures can be advantageously used in many applications requiring miniaturization and multiband waveguides, such as miniaturized multifunction antennas and filters.

## ACKNOWLEDGMENT

This research was funded by the Leading Talents of Guangdong Province Program, grant number 2016LJ06D557 and the AoShan Talents Outstanding Scientist Program supported by Pilot National Laboratory for Marine Science and Technology (Qingdao), grant number 2017ASTCP-OS03.

## REFERENCES

1. Wikström, G., et al., “Challenges and technologies for 6G,” *2020 2nd 6G Wireless Summit (6G SUMMIT)*, 1–5, Levi, Finland, 2020.
2. Kehn, M. N. M. and P. S. Kildal, “Miniaturized rectangular hard waveguides for use in multifrequency phased arrays,” *IEEE Transactions on Antennas and Propagation*, Vol. 53, No. 1, 100–109, 2005.
3. Bozzi, M., A. Georgiadis, and K. Wu, “Review of substrate-integrated waveguide circuits and antennas,” *IET Microwaves, Antennas & Propagation*, Vol. 5, No. 8, 909–920, 2011.
4. Veselago, V. G., “The electrodynamics of substances with simultaneously negative values of  $\epsilon$  and  $\mu$ ,” *Sov. Phys. Usp.*, Vol. 10, 509–514, 1968.
5. Hrabar, S., J. Bartolic, and Z. Sipus, “Waveguide miniaturization using uniaxial negative permeability metamaterial,” *IEEE Transactions on Antennas and Propagation*, Vol. 53, No. 1, 110–119, 2005.
6. Siakavara, K., “Modal analysis of the microwave frequency response and composite right-/left-handed operation of a rectangular waveguide loaded with double positive and double negative materials,” *Int. J. RF Microwave Comput. Aided Eng.*, Vol. 1, 435–445, 2010.
7. Raveu, N., B. Byrne, L. Claudepierre, and N. Capet, “Modal theory for waveguides with anisotropic surface impedance boundaries,” *IEEE Trans. Microw. Theory Techn.*, Vol. 64, 1153–62, 2016.
8. Kuhler, L., G. Le Fur, L. Duchesne, and N. Raveu, “The propagation characteristics of 2-D metamaterial waveguides using the modal expansion theory,” *IEEE Trans. Microw. Theory Techn.*, Vol. 66, 4319–26, 2018.
9. Kim, D. J. and J. H. Lee, “Beam scanning leaky-wave slot antenna using balanced CRLH waveguide operating above the cutoff frequency,” *IEEE Transactions on Antennas and Propagation*, Vol. 61, No. 5, 2432–2440, 2013.
10. Jin, J. Y., X. Q. Lin, and Q. Xue, “A miniaturized evanescent mode waveguide filter using RRRs,” *IEEE Transactions on Microwave Theory and Techniques*, Vol. 64, No. 7, 1989–1996, 2016.
11. Kehn, M. N. M., M. Nannetti, A. Cucini, et al., “Analysis of dispersion in dipole-FSS loaded hard rectangular waveguide,” *IEEE Transactions on Antennas and Propagation*, Vol. 54, No. 8, 2275–2282, 2006.
12. Rajo-Iglesias, E., Ó. Quevedo-Teruel, and M. N. M. Kehn, “Multiband SRR loaded rectangular waveguide,” *IEEE Transactions on Antennas and Propagation*, Vol. 57, No. 5, 1571–1575, 2009.
13. İbili, H., S. Keleş, Ö. Eriş, and Ö. Ergül, “Realization of multiband microwave metamaterials fabricated via low-cost inkjet printing,” *2019 European Microwave Conference in Central Europe (EuMCE)*, 35–38, Prague, Czech Republic, 2019.
14. Justin, G. P., “Analysis and design of a new class of miniaturized circular waveguides containing anisotropic metamaterial liners,” The Degree of Doctor of Philosophy’s Thesis, Dept. Elect. Comput. Eng., University of Alberta, 2016.
15. Ravelo, B. and B. Mazari, “Characterization of the regular polygonal waveguide for the RF EM shielding application,” *Progress In Electromagnetics Research M*, Vol. 12, 95–105, 2010.
16. Collin, R. E., *Field Theory of Guided Waves*, 2nd edition, IEEE Press, New York, 1991.
17. Ravelo, B., A. Thakur, A. Saini, and P. Thakur, “Microstrip dielectric substrate material characterization with temperature effect,” *ACES Journal*, Vol. 30, No. 12, 1322–1328, 2015.
18. Lewi, T., “Thermally reconfigurable meta-optics,” *IEEE Photonics Journal*, Vol. 11, No. 2, 1–16, 2019.

19. Silveirinha, M. and N. Engheta, "Tunneling of electromagnetic energy through subwavelength channels and bends using  $\varepsilon$ -near-zero materials," *Physical Review Letters*, Vol. 97, No. 15, 157403.1–157403.4, 2006.
20. Engheta, N. and R. Ziolkowski, *Metamaterials: Physics and Engineering Explorations*, Wiley, 2006.
21. Alu, A., M. G. Silveirinha, A. Salandrino, et al., "Epsilon-near-zero metamaterials and electromagnetic sources: Tailoring the radiation phase pattern," *Physical Review B, Condensed Matter and Materials Physics*, Vol. 75, No. 15, 155410.1–155410.13, 2007.